Available online at www.sciencedirect.com
SCIENCE DIRECT®
International Journal of Heat and Fluid Flow 24 (2003) 864–873
International Journal of HEAT AND FLUID FLOW
www.elsevier.com/locate/ijhff

Transient numerical simulation of buoyancy driven flow adjacent to an elliptic tube

F.M. Mahfouz [a], Serpil Kocabiyik [b,*]

[a] Mechanical Power Department, Faculty of Engineering, Menoufia University, Egypt
[b] Department of Mathematics and Statistics, Memorial University of Newfoundland, St. John's, Nfld, Canada A1C 5S7

Received 16 December 2002; accepted 19 June 2003

Abstract

In this paper the problem of laminar, transient, two-dimensional free convective heat transfer from the surface of a horizontal elliptic tube is considered. The tube, whose surface is suddenly subjected to uniform heat flux, is placed in a quiescent Boussinesq Newtonian fluid with its major axis horizontal. The details of both flow and thermal fields are obtained by solving the full governing Navier–Stokes and energy equations. These equations, expressed in terms of stream function, vorticity and temperature, are numerically solved using an implicit spectral finite difference procedure. The parameters involved are the modified Rayleigh number, Prandtl number and axis-ratio. The investigation covers a Rayleigh number range up to 10^7. The minor–major axis ratio of elliptic cylinder ranges between 0.05 and 0.998 and Prandtl number ranges between 0.1 and 10. The effects of these parameters on the surface temperature distribution and heat transfer coefficients are determined and the different aspects of the results are discussed for some selected cases.

Keywords: Free convection; Heat transfer; Elliptic tube; Boussinesq Newtonian fluid; Unsteady; Temperature; Thermal; Computation

1. Introduction

The process of free convective heat transfer from the surface of a body to the surrounding fluid is of great importance in the field of thermo-fluid mechanics. This process is of technological importance in the design of heat exchanger devices and solar collectors, and cooling of electrical and electronic components and many others. One body shape of particular importance is a cylindrical tube, and in the design of heat exchangers, special interest was directed to tubes of elliptic cross-section since they were found to create less resistance to cooling fluid which results in less pumping power.

Although in heat exchangers the forced convection is dominant, the free convection becomes the dominant mode of heat transfer in case of power failure. Moreover, elliptical tube geometry is general enough to encompass all elliptical cross-sections between the limiting cases of a circular cylinder and a flat plate which enables academic researchers to verify their results by comparing them with well known previous results for these two limiting cases (e.g. Sparrow and Gregg, 1956; Koh, 1964; Kim et al., 1975; Fujii and Imura, 1972).

As well known, in the thermo-fluid mechanics community, in buoyancy driven flow problems the thermal boundary conditions play an important role in determining both flow and thermal fields. These boundary conditions are mainly the prescribed surface temperature and the prescribed surface heat flux. In the case of prescribed surface temperature the heat transfer rate calculations and control are of main interest whereas in the case of prescribed heat flux the surface temperature distribution is of great importance. Although most of the previous studies have focused on constant surface temperature boundary condition, the case of uniform surface heating is practically important.

Relatively few theoretical and experimental studies have been carried out on problems concerning free convection from elliptic tubes. Lin and Chao (1974) investigated the steady natural convection from two-dimensional and axisymmetric isothermal bodies with an arbitrary cross-section. In their study the special cases of circular and elliptic cylinders were considered.

* Corresponding author. Tel.: +709-737-8783; fax: +709-737-3010.
E-mail address: mathstat@math.mun.ca (S. Kocabiyik).

0142-727X/$ - see front matter © 2003 Elsevier Inc. All rights reserved.
doi:10.1016/S0142-727X(03)00091-2

Nomenclature

a, b	semi-major and semi-minor axes lengths [m]
Ar	minor to major axis ratio, b/a
c'	eccentricity of the ellipse
c_v	specific heat [J kg^{-1} K^{-1}]
$F_{x'}$, $F_{y'}$	x' and y' components of the buoyancy force [N]
f_n	functions defined in (9a)
g	gravitational acceleration [m s^{-2}]
g_n	functions defined in (9b)
h, $\bar{h}$	local and average heat transfer coefficients [W m^{-2} K^{-1}]
H_0, H_n	functions defined in (9c)
k	thermal conductivity [W m^{-1} K^{-1}]
Nu, $\overline{Nu}$	local and average Nusselt numbers
P	perimeter [m]
Pr	Prandtl number (ν/α)
q	prescribed (constant) heat flux [W m^{-2}]
Ra	modified Rayleigh number $(g\beta(2a)^3 aq/k\nu\alpha)$
t	dimensional time [s]
T	dimensional temperature of fluid [K]
x, y	dimensionless Cartesian coordinates [m]
Y^*	the dimensionless distance from the tube surface [m] ($Y^* = \frac{x'-b}{2a}Ra^{0.25}$ along the line $\eta = 0$, $Y^* = \frac{y'-a}{2a}Ra^{0.25}$ along the line $\eta = 90°$)

Greeks

α	fluid thermal diffusivity [m^2 s^{-1}]
β	coefficient of volumetric thermal expansion [K^{-1}]
ε	dimensionless ratio, a/c'
ξ, η	elliptic coordinates [m]
ξ_0	constant defined by $\tanh^{-1}$ Ar
μ	dynamic viscosity [Pe s]
ν	kinematic viscosity [m^2 s^{-1}]
ρ	fluid density [kg m^{-3}]
τ	dimensionless time
Θ	dimensionless temperature, $k(T - T_\infty)/aq$
ψ	dimensionless stream function
ς	dimensionless vorticity

Subscripts

m	mean
s, o	cylinder surface
∞	infinite distance from the surface

Superscript

$'$	dimensional quantity

The study was based on the solution of boundary-layer equations which have the drawback of being non-applicable in the buoyant plume region. Raithby and Hollands (1976) studied the problem of steady natural convection from an elliptic cylinder with a vertical plate and a horizontal circular cylinder as special cases. Both isothermal and constant heat flux boundary conditions were considered with emphasis on isothermal surface cases. In their work, a thin layer analysis applicable only to thin boundary-layer flow was modified to take into consideration the effects of thick boundary layer resulting at low Rayleigh numbers. The average Nusselt numbers for steady-state flow were found to be in a good agreement with the experimental data for a wide range of Rayleigh numbers. Merkin (1977) studied the symmetrical case of the same problem for various eccentricities in both cases when the major axis was horizontal or vertical. The numerical results, based on the solution of boundary-layer equations, were presented for the cases of constant surface temperature and constant surface heat flux. The obtained results have the same drawback mentioned in the work by Lin and Chao. Huang and Mayinger (1984) investigated the steady free convection from an isothermal elliptic tubes for different orientations and for different axis ratios. The local and average Nusselt numbers were reported, together with correlations for average Nusselt number. Purely numerical studies on free convection from isothermal horizontal elliptic tubes include the work by Badr and Shamsher (1993) and Badr (1997). Both of these studies were based on the solution of full conservation equations of mass, momentum, and energy with no boundary-layer simplifications. Badr and Shamsher solved the problem of free convection from an elliptic cylinder for Rayleigh numbers ranging from 10 to 10^3, and axis ratios ranging from 0.1 to 0.964. Badr investigated the effects of the tube orientations in the axis ratio range $0.4 \leqslant \mathrm{Ar} \leqslant 0.98$ at the two Rayleigh numbers of 10^3 and 10^4. The study by Badr and Shamsher focused on the final steady-state solution with no details reported on the transient results unlike Badr's work. The most recent numerical studies on mixed convection from an elliptic tube placed in a fluctuating free stream were made by Ahmad and Badr (2001, 2002). It is noted that the velocity and temperature fields in the presence of a fluctuating free stream are different from the present case (quiescent fluid).

To our knowledge, from a survey of existing literature, there is a lack of detailed information on the free transient convection from elliptic tubes whose surface is suddenly subjected to uniform heat flux. This is the motivation of the present work in which the same

problem is considered and the unsteady full Navier–Stokes and energy equations for laminar, two-dimensional flow of Boussinesq fluid are solved.

2. Problem formulation

The problem considered is that of a long horizontal tube of an elliptic cross-section with semi-major axis length a, placed in a quiescent Boussinesq Newtonian fluid of infinite extent as shown in Fig. 1. The tube and the stagnant fluid around the tube have the same initial temperature T_∞ at time $t < 0$. At time $t = 0$ the tube surface is suddenly heated with uniform heat flux q. Right after this time the difference between the mean temperature of the tube surface and the temperature of the far-field gives rise to the buoyancy force to develop and cause the fluid motion. The tube is considered to be long enough so that the end effects can be neglected and accordingly the induced flow can be assumed two-dimensional. The viscous dissipation and the effect of temperature variation on fluid properties are considered negligible except for the body force term in momentum equation (the Boussinesq approximation).

Assuming time dependent flow in the (x', y') plane the conservation equations of mass, momentum and energy in terms of the vorticity ζ', stream function ψ' and temperature T can be written as

$$\frac{\partial \zeta'}{\partial t} + \frac{\partial \psi'}{\partial y'}\frac{\partial \zeta'}{\partial x'} - \frac{\partial \psi'}{\partial x'}\frac{\partial \zeta'}{\partial y'} = v\nabla^2\zeta' + \frac{1}{\rho}\left[\frac{\partial F_{y'}}{\partial x'} - \frac{\partial F_{x'}}{\partial y'}\right], \quad (1)$$

$$\zeta' = -\nabla^2\psi', \quad (2)$$

$$\frac{\partial T}{\partial t} + \frac{\partial \psi'}{\partial y'}\frac{\partial T}{\partial x'} - \frac{\partial \psi'}{\partial x'}\frac{\partial T}{\partial y'} = \frac{k}{\rho c_v}\nabla^2 T, \quad (3)$$

where

$$\nabla^2 = \frac{\partial^2}{\partial x'^2} + \frac{\partial^2}{\partial y'^2},$$

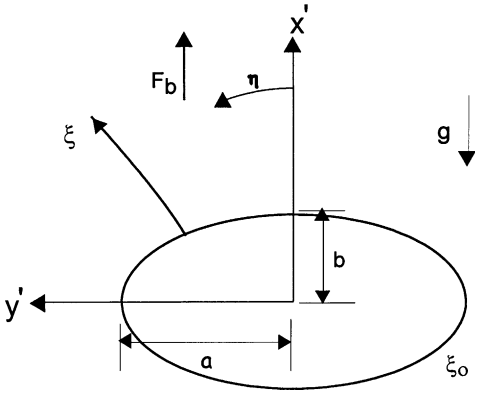

Fig. 1. Physical model and coordinate system.

$F_{x'}$, and $F_{y'}$ are the x' and y' components of the buoyancy force and defined as

$$F_{x'} = \rho g\beta(T - T_\infty) \quad \text{and} \quad F_{y'} = 0.$$

The boundary conditions are mainly the no-slip and impermeability conditions on the tube surface and the stagnant ambient conditions far away from it. The boundary condition can be expressed as

$$\psi' = \frac{\partial \psi'}{\partial x'} = 0 \quad \text{and} \quad q = -k\frac{\partial T}{\partial n} = \text{const.}$$
on the tube surface, (4a)

$$\frac{\partial \psi'}{\partial x'} \to 0, \quad \frac{\partial \psi'}{\partial y'} \to 0 \quad \text{and} \quad T \to T_\infty$$
far away from the tube surface, (4b)

where n is the dimensional coordinate normal to the surface. The dimensionless variables are related to their counterparts through

$$x = \frac{x'}{a}, \quad y = \frac{y'}{a}, \quad t = \frac{t\alpha}{a^2}, \quad \psi = \frac{\psi'}{\alpha},$$
$$\zeta = -\zeta'\frac{a^2}{\alpha} \quad \text{and} \quad \Theta = \frac{k(T - T_\infty)}{aq}.$$

For accurate numerical treatment we introduce elliptic coordinates ξ, η that are better suited for the geometry of the problem

$$\xi + \mathrm{i}\eta = \sinh^{-1}\frac{x + \mathrm{i}y}{\sqrt{1 - \mathrm{Ar}^2}}.$$

The line $\eta = 0$ coincides with the vertical line along the minor-axis of the ellipse and passes through the center of the tube cross-section as shown in Fig. 1. The surface of the elliptic tube is defined by the constant $\xi_0 = \tanh^{-1}\mathrm{Ar}$. Using the elliptic coordinate system, with the origin at the center of the tube, Eqs. (1)–(3) in dimensionless form become

$$J\frac{\partial \zeta}{\partial t} = Pr\left(\frac{\partial^2\zeta}{\partial \xi^2} + \frac{\partial^2\zeta}{\partial \eta^2}\right) + \frac{\partial \psi}{\partial \xi}\frac{\partial \zeta}{\partial \eta} - \frac{\partial \psi}{\partial \eta}\frac{\partial \zeta}{\partial \xi} + \frac{Ra\,Pr}{8\varepsilon}\left[\cosh\xi\sin\eta\frac{\partial \Theta}{\partial \xi} + \sinh\xi\cos\eta\frac{\partial \Theta}{\partial \eta}\right], \quad (5)$$

$$J\zeta = \frac{\partial^2\psi}{\partial \xi^2} + \frac{\partial^2\psi}{\partial \eta^2}, \quad (6)$$

$$J\frac{\partial \Theta}{\partial t} = \left(\frac{\partial^2\Theta}{\partial \xi^2} + \frac{\partial^2\Theta}{\partial \eta^2}\right) + \frac{\partial \psi}{\partial \xi}\frac{\partial \Theta}{\partial \eta} - \frac{\partial \psi}{\partial \eta}\frac{\partial \Theta}{\partial \xi}, \quad (7)$$

where $J = (\cosh^2\xi - \sin^2\eta)(1 - \mathrm{Ar}^2)$ is the determinant of the Jacobian of transformation matrix. The velocity components in ξ and η directions are then defined as

$$U_\eta = -\frac{1}{J^{1/2}}\frac{\partial \psi}{\partial \xi} \quad \text{and} \quad V_\xi = \frac{1}{J^{1/2}}\frac{\partial \psi}{\partial \eta}.$$

The boundary conditions (4) can now be expressed as

$$\psi = \frac{\partial \psi}{\partial \xi} = 0, \quad \frac{\partial \psi}{\partial \eta} = 0 \quad \text{and} \quad \frac{\partial \Theta}{\partial \xi} = -J^{1/2} \quad \text{at } \xi = \xi_0, \tag{8a}$$

$$\frac{\partial \psi}{\partial \xi} \to 0, \quad \frac{\partial \psi}{\partial \eta} \to 0 \quad \text{and} \quad \Theta \to 0 \quad \text{as } \xi \to \infty. \tag{8b}$$

The initial conditions (at times $t < 0$) are the stationary conditions and uniform temperature distribution ($\Theta = 0$) in the entire field. At the start of computations $t = 0$, the tube surface is suddenly heated with uniform heat flux ($\frac{\partial \Theta}{\partial \xi} = -J^{1/2}$ on the tube surface) and this moment represents the start of the time development of flow and thermal fields. The main mathematical problem is to predict the details of both fields as time increases.

3. The method of solution

The method of solution is in principle similar to that developed by Collins and Dennis (1973), and Badr and Dennis (1985). The velocity and temperature fields are symmetric about the vertical line $\eta = 0$ passing through the tube center. Accordingly the stream function ψ, vorticity ζ and temperature Θ are approximated using Fourier series expansions as

$$\psi = \sum_{n=1}^{N} f_n(\xi, t) \sin(n\eta), \tag{9a}$$

$$\zeta = \sum_{n=1}^{N} g_n(\xi, t) \sin(n\eta), \tag{9b}$$

$$\Theta = H_0(\xi, t) + \sum_{n=1}^{N} H_n(\xi, t) \cos(n\eta), \tag{9c}$$

where N is the order of truncation in the Fourier series. Substituting Eqs. (9a)–(9c) in Eqs. (5)–(7), after using simple mathematical analysis, results in the following set of differential equations

$$\frac{\partial^2 f_n}{\partial \xi^2} - n^2 f_n = \frac{1}{2\varepsilon^2}\left(\cosh 2\xi g_n - \frac{1}{2}\left[g_{(n+2)} + \operatorname{sgn}(n-2) g_{|n-2|}\right]\right), \tag{10}$$

$$\cosh 2\xi \frac{\partial g_n}{\partial t} - \frac{1}{2}\left[\frac{\partial g_{(n+2)}}{\partial t} + \operatorname{sgn}(n-2)\partial g_{|n-2|}\partial t\right] = 2\varepsilon^2 Pr\left(\frac{\partial^2 g_n}{\partial \xi^2} - n^2 g_n\right) + S_n, \tag{11}$$

$$\cosh 2\xi \frac{\partial}{\partial t}\begin{pmatrix} H_0 \\ H_n \end{pmatrix} - \frac{1}{2}\frac{\partial}{\partial t}\begin{bmatrix} H_2 \\ H_{(n+2)} \end{bmatrix} - \frac{1}{2}\frac{\partial}{\partial t}\begin{bmatrix} 0 \\ H_{|n-2|} \end{bmatrix} = 2\varepsilon^2 \frac{\partial^2}{\partial \xi^2}\begin{pmatrix} H_0 \\ H_n \end{pmatrix} - 2n^2\varepsilon^2 \begin{pmatrix} 0 \\ H_n \end{pmatrix} + \begin{pmatrix} Z_0 \\ Z_n \end{pmatrix}. \tag{12}$$

Here $\varepsilon = (1 - \mathrm{Ar}^2)^{-1/2}$, $\operatorname{sgn}(n-2)$ is the sign of term $(n-2)$ and $g_{|n-2|} = 0, H_{|n-2|} = H_0$ and $\operatorname{sgn}(n-2) = 0$ when $n = 2$. The functions S_n, Z_0 and Z_n are defined as

$$S_n = \sum_{m=1}^{N} (kf_k - jf_j)\frac{\partial g_m}{\partial \xi} - m\left(\operatorname{sgn}(m-n)\frac{\partial f_j}{\partial \xi} - \frac{\partial f_k}{\partial \xi}\right) g_m,$$

$$Z_0 = -2\sum_{n=1}^{N} n \frac{\partial}{\partial \xi}(f_n H_n),$$

$$Z_n = \sum_{m=1}^{N} (kf_k - jf_j)\frac{\partial H_m}{\partial \xi} - m\left(\operatorname{sgn}(m-n)\frac{\partial f_j}{\partial \xi} - \frac{\partial f_k}{\partial \xi}\right) H_m,$$

where $j = |m-n|$, $k = m+n$. The boundary conditions for the functions $f_n(\xi, t)$, $g_n(\xi, t)$, $H_0(\xi, t)$ and $H_n(\xi, t)$ are deduced from Eq. (8) and can be expressed as

$$f_n = \frac{\partial f_n}{\partial \xi} = 0 \quad \text{and} \quad \frac{\partial H}{2\partial \xi} + \sum_{1}^{N} \frac{\partial H_n}{\partial \xi} \cos(n\eta) = -J^{1/2} \quad \text{at } \xi = \xi_0, \tag{13a}$$

$$\frac{1}{J^{1/2}}\frac{\partial f_n}{\partial \eta}, \quad \frac{1}{J^{1/2}}\frac{\partial f_n}{\partial \xi}, \quad g_n, \quad H_0, H_n \to 0 \quad \text{as } \xi \to \infty. \tag{13b}$$

Integrating the both sides of Eq. (10) with respect to ξ, after multiplying by $e^{-n\xi}$, from $\xi = \xi_0$ to ∞ and using the boundary conditions (13), we obtain the integral condition

$$\int_{\xi_0}^{\infty} e^{-n\xi}\left(\cosh 2\xi g_n + \frac{1}{2}\left[g_{(n+2)} + \operatorname{sgn}(n-2) g_{|n-2|}\right]\right) d\xi = 0. \tag{14}$$

This condition gives a constraint on the vorticity and is used to calculate the values of the function g_n on the tube surface, instead of the gradient condition (8b), to calculate the surface vorticity distribution.

4. Numerical integration procedure

The solution procedure and the details of the numerical technique for solving Eqs. (10)–(12) subject to (13) and satisfying the integral condition (14) is based on the method developed by Collins and Dennis (1973), and Badr and Dennis (1985). Although the differential equations (10)–(12) and boundary and integral conditions are different from those used in the above mentioned works, the numerical procedure is almost the same and a brief description of the numerical method is given below.

The numerical integration of Eqs. (10)–(12) starts at $t = 0$ by setting

$$\frac{\partial H_0}{2\partial \xi} + \sum_{1}^{N} \frac{\partial H_n}{\partial \xi} \cos(n\eta) = -J^{1/2}$$

at $\xi = \xi_0$ while equating all other Fourier coefficients to zero in the entire domain. This simulates the sudden surface heating by uniform heat flux which initially results in a sudden rise of the surface temperature from T_∞ to T_s. The far field conditions at $\xi \to \infty$ are enforced at a distance that can reach a maximum of $\xi_{max} = \xi_0 + 10$, which corresponds to a very large distance away from the tube surface. Such far-away boundary ensures that the conditions at infinity are appropriately incorporated in the numerical solution. The number of points in the ξ direction is taken as 200 with a grid size taken as 0.05 for most of the cases. However, the grid size is reduced for relatively high Rayleigh number cases ($Ra > 10^5$).

The numerical scheme used for advancing the solution of ψ, ζ and Θ through one time step is in principle similar to that used given by Collins and Dennis (1973), and Badr and Dennis (1985). The only difference is the appearances of derivatives $\partial g_{(n+2)}/\partial t$, $\partial g_{|n-2|}/\partial t$ in Eq. (11). When solving for g_n, the functions with subscripts $(n+2)$ are unknown. These unknown functions $\partial g_{(n+2)}/\partial t$ are taken care by approximating their values at time $(t + \Delta t)$ to be initially the same as at time t and then updating these values through an iterative procedure. The iterative process stopped when the difference in the solution of g_n, between two successive iterations falls into a given tolerance of 10^{-6}. The integral condition was utilized to determine g_n on the tube surface. Eq. (10) is solved using a step-by-step integration scheme. A straightforward finite-difference solution for this equation results in an extremely unstable solution especially for large values of N.

Solution procedure for Eq. (12) uses an implicit method of Crank-Nicolson and is similar to that used for Eq. (11) except that boundary values of $\partial H_0/\partial \xi$, $\partial H_n/\partial \xi$ at $\xi = \xi_0$ are completely known and there are no integral conditions. The solution of the three equations (10)–(12) is repeated until a convergence criteria similar to that used for determining g_n is achieved.

To obtain reasonably accurate solution, a small time step of $\Delta t = 10^{-5}$ is considered for the first 10 time steps then is increased to $\Delta t = 10^{-4}$ for the next 10 time steps. In the rest of the solution the time step is increased to a certain value which depends on the value of Ra. The higher the Ra is the smaller the time step should be. The number of terms in Fourier series is taken as 5 terms at the start of the numerical calculations and more terms are added with the increase of the time. One more term is added at a time when the last non-zero term reaches the value of 10^{-4}. The maximum number of terms N used for most of the cases considered in this study is 40.

Once the velocity and temperature fields are calculated, the local and average Nusselt numbers as well as the mean surface temperature can be obtained. The local Nusselt number is defined as

$$Nu = 2ah/k, \tag{15}$$

where h is the local heat transfer coefficient defined as $h = q/(T_s - T_\infty)$.

Using the above definitions, the Nu can be expressed in terms of H_0 and H_n as

$$Nu = \frac{4}{H_0 + 2\sum_1^N H_n \cos(n\eta)}. \tag{16}$$

The average Nusselt number is defined as

$$\overline{Nu} = 2a\bar{h}/k,$$

where $\bar{h}$ is the average heat transfer coefficient. The average Nusselt number is related to the mean surface temperature, Θ_m by

$$\overline{Nu}\Theta_m = 2, \tag{17}$$

where Θ_m is defined as

$$\Theta_m = \frac{1}{P}\int_0^P \Theta \, dP. \tag{18}$$

Here P is the perimeter of the elliptic section.

5. Verification of the method of solution and discussion of results

The accuracy of the method of solution is verified by considering a number of cases for which theoretical results are available for comparison.

In Fig. 2, the average Nusselt number $\overline{Nu}$ results for the special case of a circular cylinder (Ar = 1) heated uniformly with constant heat flux, reported by Raithby and Hollands (1976, see p. 79, Eq. (33) and Table 6), are compared with the case of elliptic tube with axis ratio Ar = 0.998 (almost circular cylinder) considered in this study. This figure shows a good agreement between the results, with maximum percentage difference in $\overline{Nu}$ less than 7%. Fig. 3 shows the surface temperature distribution in case of Ar = 0.75 and $Pr = 1$ obtained in this study and those reported by Merkin (1977) for the three Rayleigh numbers of 10^3, 10^5 and 10^7. It is noted that Merkin's study was based on the boundary-layer approximation which may be the limiting case as $Ra \to \infty$ for laminar flow excluding the plume region. The difference between the results is clearly pronounced in the plume region near $\eta = 0$, and also in neighborhood of $\eta = 87°$ where steep surface curvature exists. At $Ra = 10^3$ (relatively low Rayleigh number), Merkin's result for the surface temperature distribution deviates significantly from the result obtained in this study with maximum percentage difference of 45% in the neighborhood of $\eta = 87°$. However, as Ra increases, the maximum percentage difference between the two results decreases. The maximum percentage difference of 20% occurs near $\eta = 87°$ at $Ra = 10^5$, whereas the maximum percentage difference of 22% occurs near $\eta = 0$ at $Ra = 10^7$.

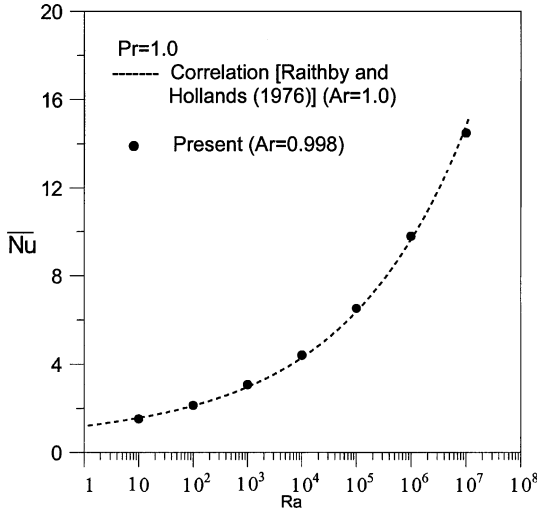

Fig. 2. Comparison between the average Nusselt number values for the range of Ra, $1.0 \leqslant Ra \leqslant 10^8$, obtained in this study (Ar = 0.998) and the results given by Raithby and Hollands (1976) for a circular cylinder (Ar = 1.0).

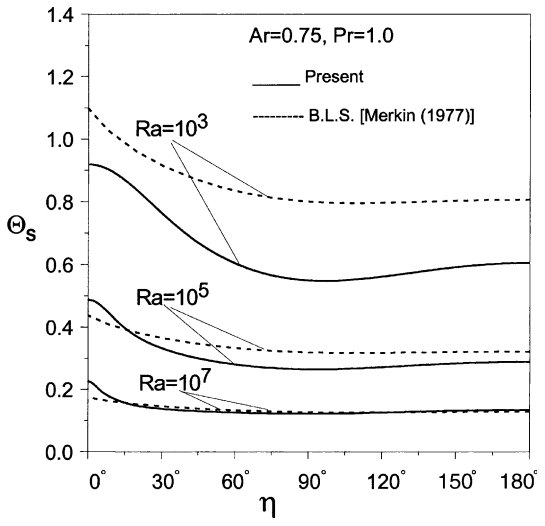

Fig. 3. Comparison of the temperature distribution along the ellipse surface obtained in this study with the boundary-layer solution (BLS) results given by Merkin (1977) for the case of Ar = 0.75 and $Pr = 1.0$ at $Ra = 10^3$, 10^5, 10^7.

The numerical results of the surface temperature distribution obtained in this study are also compared with Merkin's results for the case of $Ra = 10^7$ and $Pr = 1$ at the three different axis ratio Ar = 0.25, 0.5 and 0.75 as shown in Fig. 4. At such relatively high Ra the agreement between the two solutions is quite good at all points except in the aforementioned two regions, namely near $\eta = 87°$ and $\eta = 0$. The figure also indicates that with the increase of Ar, the agreement between the two solutions improves in the neighborhood of $\eta = 87°$. On the other hand, the increase of Ar has a reverse effect on

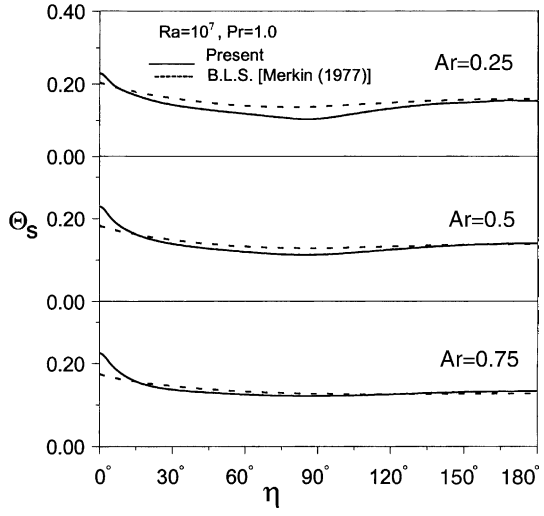

Fig. 4. Comparison of the temperature distribution along the ellipse surface obtained in this study with the boundary-layer solution (BLS) results given by Merkin (1977) for the case of $Ra = 10^7$ and $Pr = 1.0$ at Ar = 0.25, 0.5, 0.75.

this agreement in the buoyant plume region near $\eta = 0$. That is as Ar increases from 0.25 to 0.75 the percentage difference between the results (i) decreases from 34% to 4% (in the region near $\eta = 87°$) and (ii) increases from 11% to 22% (in the region near $\eta = 0$).

In the following, we will present results for a range of modified Rayleigh number up to 10^7, a range of Prandtl number between 0.1 and 10 and a range of axis ratio between 0.05 and 0.998. Fig. 5 shows the time variation of average Nusselt number $\overline{Nu}$ for the case of $Ra = 10^4$ and Ar = 0.5 and at the three Prandtl numbers of 0.1, 1.0, 10. The figure clearly shows that the general variation of Nusselt number is similar to that for isothermal elliptic and/or circular tube (see for example Mahfouz and Badr, 1999). As expected, $\overline{Nu}$ takes very high values at small times since the thermal layer starts with small thickness following the sudden tube surface heating. The sharp decrease in $\overline{Nu}$ at small times reflects the rapid growth of the thermal layer. The conduction mode of heat transfer at this early time stages dominates due to the negligibly small flow velocities. As the time goes, the decrease in $\overline{Nu}$ continues until it reaches its steady value at a certain time. The transition from conduction mode domination to convection mode domination takes the form of overshoot in a average heat transfer coefficient (i.e. in $\overline{Nu}$). At later times the buoyancy force effect prevails with $\overline{Nu}$ gradually approaching the steady-state value. In Fig. 6 the time variation of mean surface temperature Θ_m is shown for the same cases presented in Fig. 5. Since the heat flux at the tube surface is constant the mean surface temperature are inversely related as stated in Eq. (17). As expected, Figs. 5 and 6 indicate that the effect of increase in the average heat transfer coefficient (or in $\overline{Nu}$) is to decrease the steady-state mean

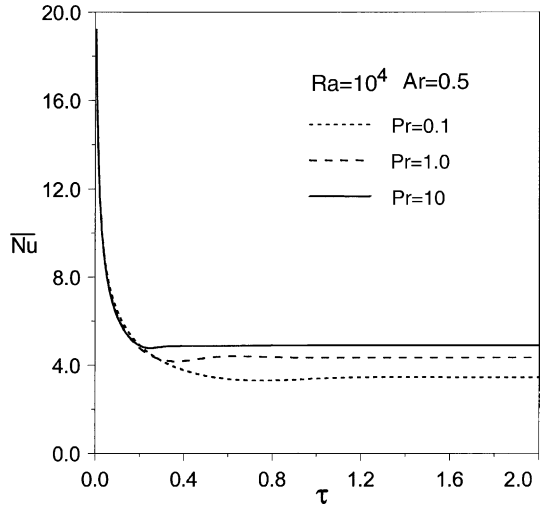

Fig. 5. The effect of Prandtl number on the time variation of the average Nusselt number for the case of $Ra = 10^4$ and Ar = 0.5.

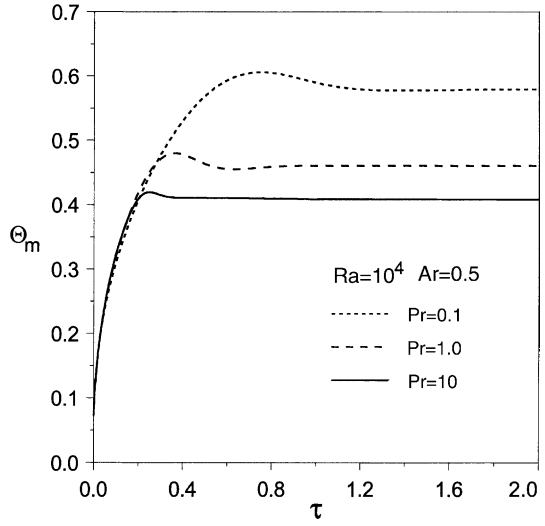

Fig. 6. The effect of Prandtl number on the time variation of mean surface temperature for the case of $Ra = 10^4$ and Ar = 0.5.

temperature as the tube surface temperature gets cooled (or as *Pr* increases) when $Ra = 10^4$ and Ar = 0.5. It is noted that in a recent work by Aydin and Guessous (2001) a dimensionless parameter is introduced for the correlation of the heat transfer in natural convection from uniformly heated vertical plate in the case of a constant wall heat flux. This dimensionless parameter depends on the Prandtl number and Rayleigh number. In their work dimensional arguments in terms of the boundary layer lead to a $Nu \sim [Ra/(1 + Pr^{-1})]^{1/5}$ dependence for the laminar heat transfer case which is consistent with existing published data (see for example Bejan, 1995; Chen and Wang, 1996).

Table 1 summarizes the effects of Rayleigh number, *Ra*, Prandtl number, *Pr*, and axis ratio, Ar, on the steady-state mean surface temperature Θ_m. The results of Table 1 shows that effect of increase of *Ra* is to decrease the steady-state mean surface temperature for fixed values of both *Pr* and Ar. This is expected since with the increase of *Ra*, convection current intensity increases, leading to a decrease in Θ_m. It is noted that Θ_m decreases with the increase of *Pr* for fixed values of both *Ra* and Ar.

Table 1
Effect of Rayleigh number *Ra*, axis ratio, Ar, and Prandtl number, *Pr* on mean surface temperature Θ_m

Ar	*Pr*	Θ		
		$Ra = 10^3$	$Ra = 10^4$	$Ra = 10^5$
0.25	0.1	0.887	0.638	0.448
	1	0.697	0.490	0.332
	10	0.631	0.435	0.290
0.5	0.1	0.813	0.579	0.394
	1	0.663	0.461	0.310
	10	0.595	0.408	0.273
0.75	0.1	0.798	0.562	0.384
	1	0.656	0.451	0.304
	10	0.587	0.401	0.268

The effect of tube axis ratio on the local Nusselt number distribution is shown in Fig. 7 for the case of $Ra = 10^5$ and $Pr = 1$. Tubes with smaller axis ratio have higher *Nu* values in the range of $\eta = 60°$–$120°$ while the differences are relatively small on the rest of the tube. All the curves in Fig. 7 posses a minimum at the topmost point on the tube surface ($\eta = 0$). As η increases from topmost point ($\eta = 0$), *Nu* increases for all values of Ar, reaching a maximum and then gradually decreases till the forward stagnation point at $\eta = 180°$. The only exception in the case of Ar = 0.998 where *Nu* continues to increase reaching its maximum value at $\eta = 180°$. It is

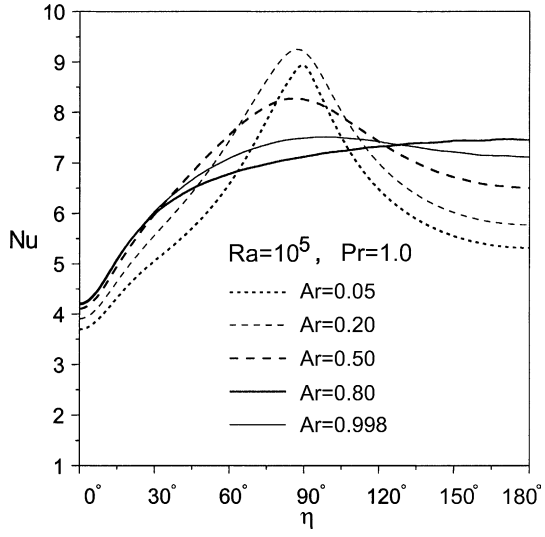

Fig. 7. The effect of axis ratio on the local Nusselt number distribution along the ellipse surface for the case of $Ra = 10^5$ and $Pr = 1.0$.

noted that with the increase of Ar not only the maximum value gets smaller but also the rate of decrease in *Nu* toward the front stagnation decreases. This leads to an increase in *Nu* at $\eta = 180°$ as Ar increases. Fig. 8 shows the surface temperature distribution, Θ_s, for the same cases presented in Fig. 7. This figure verifies that there is an inverse relationship between Θ_s and *Nu* as shown in Fig. 7. Thus the surface temperature reaches its minimum value at the point of maximum heat transfer coefficient (i.e. maximum *Nu*). Also, the effect of decrease of Ar is to decrease the steady mean surface temperature.

Fig. 9 shows the steady-state temperature decay along the extension of ellipse major axis ($\eta = 0°$) and minor axis ($\eta = 90°$) for the case of $Ra = 10^4$ and $\mathrm{Ar} = 0.5$ at the three Prandtl numbers of 0.1, 1.0, 10. The temperature gradient at the tube surface $Y^* = 0$ at the two end of both minor and major axis ($\eta = 0°$, $\eta = 90°$) is the same for fixed *Pr*. This confirms the fact that the heat flux is constant. Also, as *Pr* increases the temperature at the tube surface decreases as a result of increasing heat transfer coefficient. Moreover, slow temperature decay within the plume region is observed along the minor axis ($\eta = 0°$) whereas the decay along the major axis $\eta = 90°$ is much faster, showing a thinner thermal boundary layer along $\eta = 90°$. However, as *Pr* increases the thermal boundary layer becomes thinner resulting in much faster temperature decay along $\eta = 90°$. The velocity distribution in η direction along the ellipse major axis $\eta = 90°$ is also shown in Fig. 10 for the same case presented in Fig. 9. The figure shows that the velocity increases rapidly near the surface until it attains a maximum value and then decreases, approaching the zero value far away from the surface. This distance at which the velocity approaches zero value

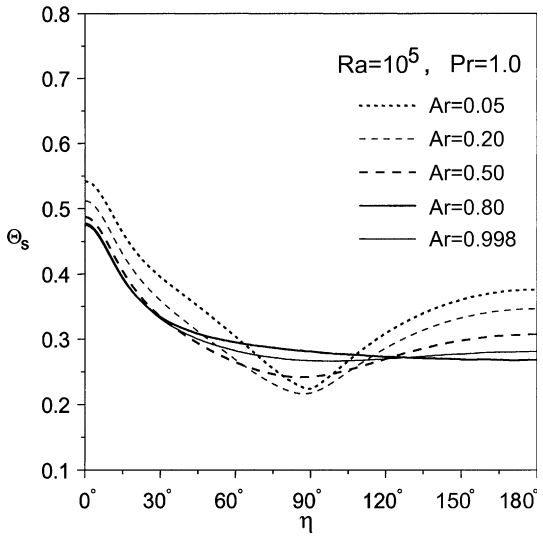

Fig. 8. The effect of axis ratio on the temperature distribution along the ellipse surface for the case of $Ra = 10^5$ and $Pr = 1.0$.

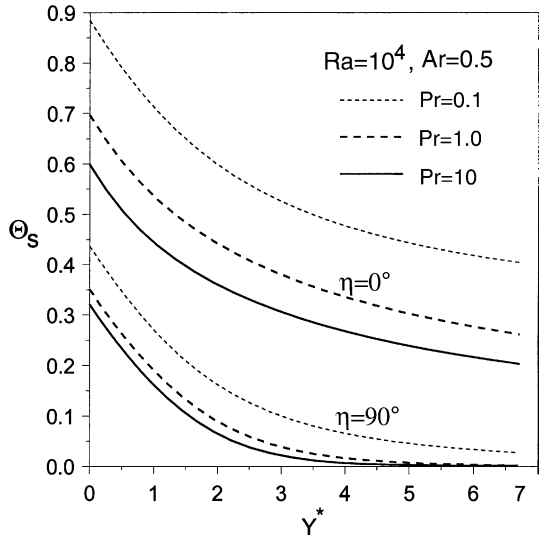

Fig. 9. The effect of Prandtl number on the temperature distribution with distance along the minor axis ($\eta = 0°$) and along the major axis ($\eta = 90°$) for the case of $Ra = 10^4$ and $\mathrm{Ar} = 0.5$.

increases as *Pr* increases as a result of increasing the boundary-layer thickness.

Fig. 11 shows the effect of *Pr* on the streamline and isotherm patterns following a sudden tube heating for the case of $Ra = 10^4$ and $\mathrm{Ar} = 0.5$ at $t = 1$ when the thermal field in the vicinity of the tube surface almost reaches the steady state. This figure verifies that at higher values of *Pr* the thermal boundary layer gets thinner and the flow field approaches to the steady state very rapidly as it was observed in Fig. 6. The streamline and isotherm patterns are shown in Fig. 12 for the case of $Ra = 10^5$, $Pr = 1.0$ and the three axis ratios of 0.25,

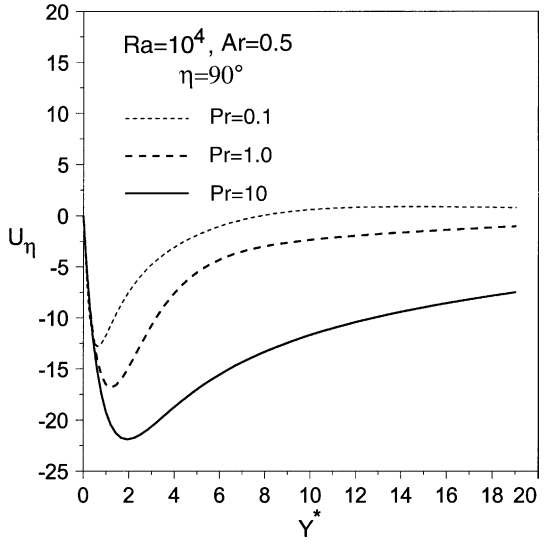

Fig. 10. The η-velocity component distribution with distance along the major axis ($\eta = 90°$) for the case of $Ra = 10^4$, $\mathrm{Ar} = 0.5$ and at $Pr = 0.1$, 1.0, 10.

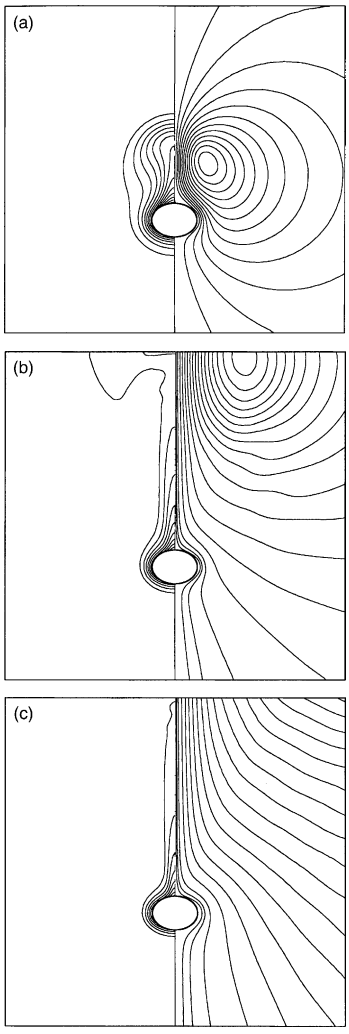

Fig. 11. The streamlines (right) and isotherms patterns (left) at time $t = 1$ for the case of $Ra = 10^4$ and Ar = 0.5: (a) $Pr = 0.1$, (b) $Pr = 1.0$, (c) $Pr = 10$.

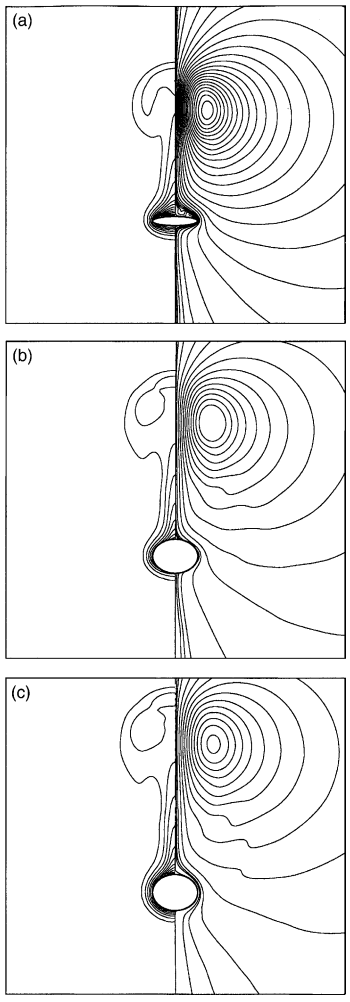

Fig. 12. The streamlines (right) and isotherms patterns (left) at time $t = 0.6$ for the case of $Ra = 10^5$ and $Pr = 1.0$: (a) Ar = 0.25, (b) Ar = 0.5, (c) Ar = 0.75.

0.5 and 0.75 at $t = 0.6$. The figure shows that the effect of the axis ratio on the streamlines and isotherms especially near the tube surface. At Ar = 0.25 the flow separation from the tube surface is observed. On the other hand there is no flow separation for the axis ratios of Ar = 0.5 and 0.75. Also, axis ratio seems to have no effects on the flow and the thermal fields far away from the tube surface. Moreover, the patterns of Fig. 12 shows that as the ellipse gets thinner the flow resistance increases, resulting in a decrease in average heat transfer coefficient (i.e. an increase of mean surface temperature). This is consistent with the results of Table 1.

6. Conclusions

The problem of laminar free convection from a horizontal tube of elliptic cross-section is investigated when the tube is suddenly heated with uniform flux. The tube is placed in an initially quiescent fluid of infinite extent. The full governing equations of motion and energy are solved in order to predict the details of the velocity and thermal boundary layers. The study is focused on the effects of modified Rayleigh number, Prandtl number and axis ratio. The results are obtained in the ranges of Rayleigh number $10^3 \leqslant Ra \leqslant 10^7$, Prandtl number $0.1 \leqslant Pr \leqslant 10$ and axis ratio $0.05 \leqslant \mathrm{Ar} \leqslant 0.998$. The method of solution is verified by comparing the average Nusselt number as well as the surface temperature distribution with the available theoretical data. The agreement is found to be satisfactory. The details of the velocity and thermal boundary layers are obtained and accordingly the velocity distribution at a given section; average Nusselt number as well as mean temperature distributions are determined for various cases. In addition the variations of vorticity, the local Nusselt number and temperature distribution are calculated over the cylinder surface. The streamlines and isotherms patterns are plotted for different Rayleigh numbers to show some

details of the velocity and temperature fields. This study reveals that the average Nusselt number increases with the increase of Rayleigh number and/or Prandtl number, resulting in a decrease in mean surface temperature. The results are also examined at high Rayleigh numbers and it is observed that the buoyancy driven flow separates from the tube surface at low values of Prandtl number when the axis ratio is small.

Acknowledgements

The support of the Natural Sciences and Engineering Council of Canada for this investigation is gratefully acknowledged.

References

Ahmad, E.H., Badr, H.M., 2001. Mixed convection from an elliptic tube placed in a fluctuating free stream. Int. J. Eng. Sci. 39, 669–693.

Ahmad, E.H., Badr, H.M., 2002. Mixed convection from an elliptic tube at different angles of attack placed in a fluctuating free stream. Heat Transfer Eng. 23, 45–61.

Aydin, O., Guessous, L., 2001. Fundamental convection for laminar and turbulent free convection from a uniformly heated vertical plate. Int. J. Heat Mass Transfer 44, 4605–4611.

Badr, H.M., 1997. Laminar natural convection from an elliptic tube with different orientations. ASME J. Heat Transfer 119, 709–718.

Badr, H.M., Dennis, S.C.R., 1985. Time-dependent viscous flow past an impulsively started rotating and translating circular cylinder. J. Fluid Mech. 158 (1985), 447–488.

Badr, H.M., Shamsher, K., 1993. Free convection from an elliptic cylinder with major axis vertical. Int. J. Heat Mass Transfer 36, 3593–3602.

Bejan, A., 1995. Convection Heat Transfer, second ed. Wiley, New York, NY.

Chen, Y.M., Wang, K.C., 1996. Numerical and experimental studies on natural convection from horizontal elliptic cylinder. J. Chin. Inst. Chem. Eng. 27, 353–362.

Collins, W.M., Dennis, S.C.R., 1973. Flow past an impulsively started circular cylinder. J. Fluid Mech. 60, 105–127.

Fujii, T., Imura, H., 1972. Natural convection heat transfer from a plate with arbitrary inclination. Int. J. Heat Mass Transfer 15, 755–761.

Huang, S.Y., Mayinger, F., 1984. Heat Transfer with natural convection around elliptic tubes. Wärm- und stoffübrtragung 18, 175–183.

Kim, C.B., Pontlkes, T.J., Wollershiem, D.E., 1975. Free convection from a horizontal cylinder with isothermal and constant heat flux surface conditions. ASME J. Heat Transfer 97, 129–130.

Koh, J.C.Y., 1964. Laminar free convection from a horizontal cylinder with prescribed surface heat flux. Int. J. Heat Mass Transfer 7, 351–354.

Lin, F.N., Chao, B.T., 1974. Laminar free convection over two dimensional and axisymmetric bodies of arbitrary contour. ASME J. Heat Transfer 96, 435–442.

Mahfouz, F.M., Badr, H.M., 1999. Heat convection from a horizontal cylinder performing steady or oscillatory rotary motion, part I steady rotation. J. Heat Mass Transfer 34, 365–373.

Merkin, J.H., 1977. Free convection boundary layers on cylinders of elliptic cross section. ASME J. Heat Transfer 99, 453–457.

Raithby, G.D., Hollands, K.G.T., 1976. Laminar and turbulent free convection from elliptic cylinders with a vertical plate and horizontal circular cylinder as special cases. ASME J. Heat Transfer 98, 72–80.

Sparrow, E.M., Gregg, J.L., 1956. Laminar free convection from a vertical plate with uniform heat flux. ASME J. Heat Transfer 75, 435–440.